Faculty Publications -- Chemistry Department   Published Research - Department of Chemistry

2014

Influence of nanostructured ceria support on platinum nanoparticles for methanol electrooxidation in alkaline media

Yunyun Zhao
University of Nebraska-Lincoln

Christian L. Menendez
University of Puerto Rico

Maxime J.-F. Guinel
University of Puerto Rico

Elizabeth C. Needels
University of Nebraska-Lincoln

Ileana Gonzalez-Gonzalez
University of Puerto Rico

See next page for additional authors

Authors

Yunyun Zhao, Christian L. Menendez, Maxime J.-F. Guinel, Elizabeth C. Needels, Ileana Gonzalez-Gonzalez, Dichele L. Jackson, Neil J. Lawrence, Carlos R. Cabrera, and Chin Li Cheung

Influence of nanostructured ceria support on platinum nanoparticles for methanol electrooxidation in alkaline media†

Yunyun Zhou,[a] Christian L. Menéndez,[b] Maxime J.-F. Guinel,[bc] Elizabeth C. Needels,[a] Ileana González-González,[b] Dichele L. Jackson,[a] Neil J. Lawrence,[a] Carlos R. Cabrera*[b] and Chin Li Cheung*[a]

The catalytic activity of platinum (Pt) nanoparticles (NPs) towards methanol electrooxidation in alkaline media was demonstrated to be dependent on their interactions with their nanostructured ceria support. Ceria nanorods (NRs) with diameters of 5 to 10 nm and lengths of 15 to 50 nm as well as ceria NPs with diameters of 2 to 6 nm were applied as supports for similarly sized Pt NPs with diameters of 2 to 5 nm. Cyclic voltammetry data showed that Pt NPs supported on ceria NPs exhibited a 2-to-5-fold higher catalytic current density *versus* ceria NRs. X-ray photoelectron spectroscopic data indicated that Pt NPs deposited onto ceria NRs were disproportionally composed of oxidized species (Pt^{2+}, Pt^{4+} and Pt−O−M) rather than Pt^0 while Pt NPs on ceria NPs mainly consisted of Pt^0. Stronger metal-support interactions between Pt NPs and ceria NRs are postulated to induce preferential oxidation of Pt NPs and consequently decrease the catalytic sites and overall activity.

1. Introduction

Development of an economically viable catalyst is essential to chemical conversion based energy production using portable fuel cells for large-scale applications such as aeronautical and space explorations.[1] A cost-effective fuel source reduces the dependence on conventional fuels required for the perpetuation of air or space transportation.[2,3] Methanol is considered as an excellent energy source for fuel cells because of its relatively high energy density (6.09 kWh kg^{-1}), ease of storage and delivery as well as its low cost synthesis from abundant natural gas resources.[4,5] Previous studies of methanol oxidation have been performed using anode catalysts such as carbon-supported platinum (Pt) modified with ceria,[6] platinum,[6] platinum-nickel oxide on carbon,[7,8] and Pt modified with rubidium.[9] Pt-based catalysts, often designed with supported nanosized Pt particles for increased effective catalytic surface areas, are one category of the most studied electrocatalyts for direct methanol fuel cells due to their high catalytic activity.[10–13]

The use of platinum in acidic electrooxidation conditions for direct alcohol fuel cells has been widely investigated using cyclic voltammetry due to its efficient oxidation of methanol.[6] However, most current research in electrooxidation of methanol has moved away from using acid media to alkaline media due to several reasons. First, some metal oxides used for supporting the platinum, such as ceria, are thermodynamically more stable in alkaline conditions.[14] They are often unstable in acidic media and tend to dissolve into metal ions.[15] Second, alkaline media can provide more sustainable conditions in industrial applications with increased power density.[16] In addition, the potential peak area overlap for the oxidation of methanol and reduction of Pt peaks further enables the possibility of using one potential to generate a larger current than the case under acidic condition.[17] Nevertheless, the performance stability of commonly used Pt-based fuel cell catalysts are still limited in both alkaline and acid media due to the poisoning of platinum by side-products (*e.g.* carbon monoxide, carbonaceous species) formed during the methanol oxidation process.[17] Various oxide promoters with high oxidizing power such as ceria[6] and nickel oxide[7] have been applied as supports for Pt NPs in order to remove catalyst poisons by oxidation and/or promote the formation of Pt^0 state on the surface of these NPs.

Ceria is a common catalyst support for Pt-based direct alcohol fuel cells because of its ability to oxidize the catalyst-poisoning carbon monoxide produced in alcohol oxidation reactions.[18–20] Nanostructured ceria of various shapes (NPs, NRs, nanotubes and mesoporous structures) have been shown to enhance the catalytic activities of metal NPs towards carbon

[a]Department of Chemistry, University of Nebraska-Lincoln, Lincoln, NE 68588, USA. E-mail: ccheung2@unl.edu

[b]Department of Chemistry and NASA-URC, Center for Advanced Nanoscale Materials, University of Puerto Rico, San Juan, Puerto Rico 00936-8377, USA. E-mail: carlos.cabrera2@upr.edu

[c]Department of Physics, College of Natural Sciences, University of Puerto Rico, San Juan, Puerto Rico 00936-8377, USA

† Electronic supplementary information (ESI) available: CVs for H-adsorption and oxidation to determine Pt active surface area and fitting parameters of XPS spectra of Pt/ceria NRs and NPs are included. See DOI: 10.1039/c3ra45829f

monoxide oxidation, the water gas shift reaction and reforming reactions at low temperatures.[21–23] The differences in their activities have been attributed to the ceria crystal plane facets,[24] density of oxygen vacancy sites[21] and crystallinity[25] of the ceria component. However, little is known about the size and plane-facet effect of ceria support in affecting these supported Pt NPs structure and their resulting catalytic activity in methanol electrooxidation. Therefore, morphological and chemical studies of nanostructured ceria and Pt NPs are necessary to elucidate the relationship between the catalytic activity and the ceria support.

Herein, we report our study of nanostructured ceria supports on the influence of the electrocatalytic activity of Pt NPs towards methanol oxidation in alkaline media. Nanostructured ceria in the form of NRs and NPs with comparable diameters and surface areas were used as supports for Pt NPs with a 20 wt% Pt loading. Transmission electron microscopy (TEM) and X-ray photoelectron spectroscopy (XPS) were applied to elucidate the size, shape and chemical state of the deposited Pt NPs on these ceria supports. Cyclic voltammetry (CV) and chronoamperometry (CA) were applied in the half-cell studies of anodes coated with these two catalysts for investigating their effectiveness in methanol oxidation.

2. Experimental method

2.1 Chemicals

Ceria (CeO_{2-x}, $0 \leq x < 0.5$) NPs were purchased from Nanoscale Inc. (Manhattan, KS). Cerium(III) sulfate hydrate ($Ce_2(SO_4)_3 \cdot xH_2O$), platinum acetylacetonate ($Pt(C_5H_7O_2)_2$) and sodium hydroxide (NaOH) were purchased from Sigma-Aldrich (St. Louis, MO). Hydrogen peroxide 30% (H_2O_2) was purchased from VWR SP (Batavia, IL). Fumion® was obtained from FuMA-Tech GmbH (St. Ingbert, Germany). All chemicals were used without further purification unless otherwise noted. A Millipore Synergy system was used to produce the deionized (DI) water of 18 MΩ cm resistivity.

2.2 Catalyst preparation

Two types of nanostructured ceria (CeO_{2-x}, $0 \leq x < 0.5$), ceria NPs and NRs, supported Pt NPs (loading: 20 wt% Pt) catalysts were studied. Ceria NPs of *ca.* 2 to 6 nm were purchased from a commercial vendor. Ceria NRs with dimensions of about 5 to 10 nm in diameter and 15 to 50 nm in length were synthesized using our previously published procedure.[21] In the ceria NRs synthesis process, 0.5 g of $Ce_2(SO_4)_3 \cdot xH_2O$ and 40 mL of 10 M NaOH were mixed and added to a 50 mL capacity Teflon-lined stainless steel autoclave. The chemicals in the autoclave were hydrothermally treated for 15 h. at 120 °C in a convection oven to generate cerium(III) hydroxide ($Ce(OH)_3$) nanorods. The product was filtered with a 3.0 μm pore size polycarbonate filter membrane (Millipore, Billerica, MA), rinsed with three aliquots of 50 mL water and placed in the convection oven for an initial oxidation at 50 °C for 2 h. During this oxidation process, most $Ce(OH)_3$ was converted to cerium oxide composed of both Ce_2O_3 and CeO_{2-x}. Then, 25 mL of 30% aqueous H_2O_2 was added to the mixture and sonicated for 30 min, followed by stirring for 30 min to allow the

reaction to reach completion. After stirring, the resulting catalyst was filtered with a 3.0 μm pore size polycarbonate membrane, rinsed with 50 mL of water and dried for 4 h. at 50 °C in a convection oven. Afterwards, the synthesized material was activated at 400 °C in simulated air (20% O_2, 80% N_2) at 100 standard cubic centimeters per minute for 30 min in a horizontal quartz tube annealing furnace with an operating pressure of 2.0 Torr.

The deposition of 20 wt% Pt NPs on ceria support was achieved by sonicating a mixture of 30 mg ceria (NRs or NPs) with 9 mL of ethanol and 6 mL of glacial acetic acid for 30 min, followed by an addition of 15.12 mg of platinum acetylacetonate, subsequent sonication for 30 min, and then heating with stirring at 100 °C until dry.[26] The product was finally activated at 400 °C in nitrogen at 1.0 Torr for 30 min.

2.3 Physical characterization method

The crystal structures of catalysts were determined using powder X-ray diffraction (XRD) (Bruker Discover D8) with a Cu K$_\alpha$ source of an average wavelength of 1.544 Å. TEM images of the catalysts were recorded using a JEOL JEM-2200FS operated at 200 kV. The TEM images were recorded either in bright field TEM mode or in scanning TEM (STEM) mode using the high-angle annular dark-field (HAADF) detector. The chemical composition of the catalyst and the oxidation states of elements in the catalyst were determined using XPS performed in a PHI 5600ci spectrometer with a hemispherical electron analyzer. A monochromatic Al K$_\alpha$ X-ray source operated at 15 kV and 350 W was used. All the recorded binding energies were calibrated using the carbon 1s peak at 284.15 eV. Pt 4f XPS data fitting analysis was performed with the software XPSPEAK. Elemental analysis of the bulk samples were performed using a Thermo Jarrell Ash IRIS Advantage inductively coupled plasma optical emission spectroscopy (ICP-OES). Typically, 25 mg of catalyst was dissolved in 10 mL of freshly made aqua regia (70% concentrated HCl: 30% concentrated HNO_3) at 110 °C for 1 h. in an acid digestion autoclave. The obtained solution was further diluted with water to a 25 mL total volume solution for the elemental analysis. The surface areas of nanostructured ceria were measured by the Brunauer–Emmett–Teller (BET) method (ASAP 2010).

2.4 Electrochemical property characterization

Pt/ceria catalyst coated glassy carbon (GC) electrodes were prepared for methanol oxidation evaluations. Typically, 8 μL of a catalyst "ink" paste consisting of 1 mg of a Pt/ceria catalyst suspended in a 100 μL Fumion® (5% w/w polyarylene sulfonic acid polyelectrolyte dissolved in water/isopropanol) was deposited onto a GC electrode and allowed to dry for 1 h.

The electrochemical characterization of the Pt/CeO_{2-x} modified electrodes material was performed under ambient conditions using cyclic voltammetry and chronoamperometry in alkaline media using a potentiostat system (Model number 1240B, CH Instruments, Inc. Austin, TX). Catalyst coated glassy carbon working electrode, Ag/AgCl reference electrode and a platinum counter electrode were arranged in a typical three-electrode half-cell configuration. All electrolyte solutions were bubbled with argon gas for 10 min before the experiments

were carried out. The surface areas of platinum on the anodes were calculated using the hydrogen adsorption/oxidation potential region from the cyclic voltammograms in an alkaline medium (0.50 M KOH solution). Cyclic voltammetry was performed at a scan rate of 100 mV s^{-1} between -0.500 V and 0.250 V vs. Ag/AgCl in 1.0 M methanol/0.50 M KOH aqueous solution at room temperature. The onset potential for each catalyst was determined at 5% of the maximum anodic peak current density for the methanol oxidation reaction at a scan rate of 1 mV s^{-1}. Chronoamperometry experiments for Pt/ceria NRs and NPs were carried out with an applied potential of -0.350 V vs. Ag/AgCl in 1.0 M methanol/0.50 M KOH aqueous solution at room temperature. The current density was normalized by the weight of Pt loading. All electrochemical impedance spectroscopy (EIS) experiments were done in an Autolab Potentiostat/Galvanostat EGSPAT 12/30. A 1.0 M methanol/0.50 M KOH solution was used for methanol oxidation studies at an applied potential of -0.400 V vs. Ag/AgCl for both catalysts. EIS was performed using a sine wave with an amplitude of 10 mV in the frequency range from 100 kHz to 1 MHz.

3. Results and discussion

3.1 Structural and chemical composition characterization of Pt/ceria NRs and NPs

3.1.1 Crystal structure and chemical composition identification of Pt/ceria NRs and NPs.
To identify the crystal structures of ceria supports and Pt crystals, both Pt/ceria NRs and NPs were characterized by XRD. The XRD patterns of ceria supports displayed diffraction peaks corresponding to those of the fluorite structured cubic ceria ($Fm\bar{3}m$, JCPDS 00-34–0394). The Pt nanoparticles present in the catalyst were found to be $Fm\bar{3}m$ cubic platinum from the XRD peaks indexed against the ICDD reference (ICDD 00-004-0802) (Fig. 1). The elemental compositions measured by ICP-OES confirmed that both catalysts contained an average of 20–24 wt% Pt. The BET data indicated that before the Pt deposition step, the ceria NRs and NPs had similar initial surface areas (90 m^2 g^{-1} vs. 83 m^2 g^{-1}).
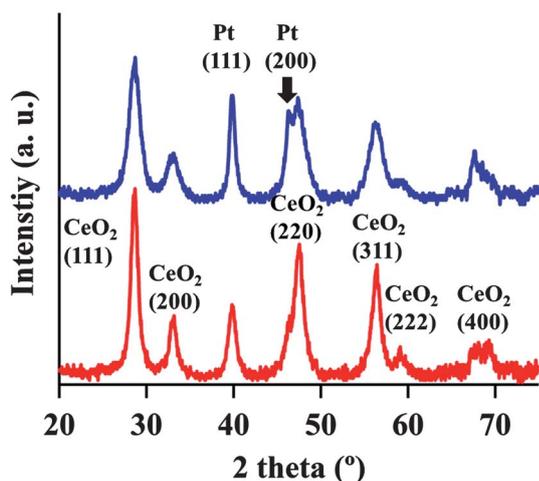

Fig. 1   X-ray diffraction patterns of (top) Pt/ceria NPs catalyst and (bottom) Pt/ceria NRs catalyst.

3.1.2 Morphology and chemical state study of Pt/ceria NRs.
The STEM-HAADF images of Pt/ceria NRs showed uniform dispersions of Pt NPs on the ceria support (Fig. 2a). The chemical contrast in the STEM images between ^{58}Ce and ^{78}Pt (Pt appears brighter) allowed for locating the Pt NPs. The diameter of Pt NPs was about 2 to 5 nm. The lengths and diameters of ceria NRs were 21.5 $\pm$ 8.5 nm and 7.3 $\pm$ 1.4 nm, respectively. Fig. 2b shows a typical TEM image of the product that mainly contained faceted and "hemispherically" shaped Pt nanocrystals. Side view images usually displayed solid anchoring of Pt NPs on ceria NRs as indicated by their faceted "hemispherical" shapes, suggesting a strong inter-diffusion between the Pt NPs and ceria. For examples, Fig. 2b shows a Pt NP anchored on a ceria NR which grew along the $\langle 110 \rangle$ direction. Two Pt NPs anchored on the tip of a nanorod are shown in Fig. 2c. The images in Fig. 2d and e are typical and indicate that Pt NPs were solidly anchored on the NR surfaces. Indeed, a good anchorage of the Pt NPs is beneficial to avoid their agglomeration and segregation.

The XPS Ce 3d binding energy region for Pt/ceria NRs suggests the presence of Ce^{3+} and Ce^{4+} species (see Fig. 3a). The Ce 3d spectrum was composed of two multiplets (v and u). These multiplets correspond to the spin–orbit split of 3d$_{5/2}$ and 3d$_{3/2}$ core electrons. The peaks labeled with v^0, v$'$, u^0 and u$'$ are indicative of Ce^{3+} peaks as opposed to those at v, v$''$, v$'''$, u, u$''$ and u$'''$ indicating the presence of Ce^{4+} states.[27] The XPS
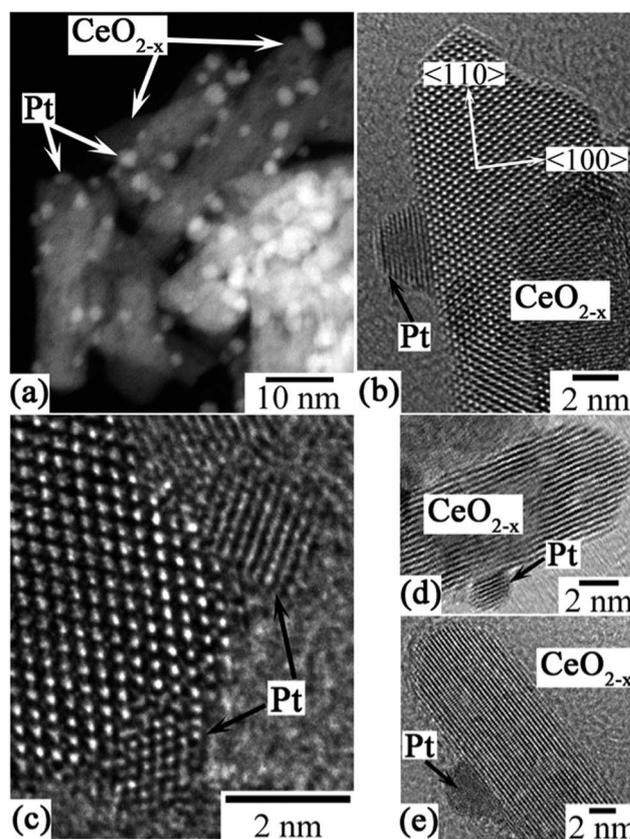

Fig. 2   (a) STEM HAADF and (b, c, d and e) TEM images of the Pt/ceria NRs catalyst.
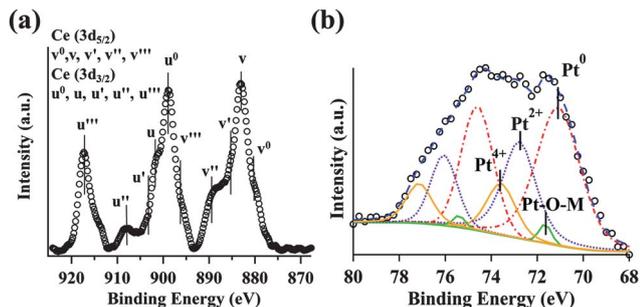
Fig. 3 X-ray photoelectron spectra and analysis of (a) Ce 3d and (b) Pt 4f binding energy regions for Pt/ceria NRs.

spectrum of Pt/ceria NRs has two spin-orbit splitting doublets Pt $4f_{7/2}$ and $4f_{5/2}$. The peaks at 71.1 and 72.8 eV binding energies are attributed to Pt^0 and Pt^{2+} states, respectively[28] (Fig. 3b). The peak at 71.7 eV is ascribed to Pt–O–M peak which corresponds to slightly ionized Pt. M has been assigned to be either a Ce cation or an oxygen vacancy site.[25] The Pt 4f spectrum fitting indicated that the Pt NPs were composed of Pt^0 and a significant portion of Pt^{2+} and Pt^{4+} states. 53% of all Pt species in Pt/ceria NRs catalyst are in the Pt^0 state, whereas the other 47% species were composed of Pt–O–M, Pt^{2+} and Pt^{4+}. (See the fitting parameters in ESI Table S1†) The formation of higher oxidation states of Pt necessitates charge transfer from the Pt to ceria support and indirectly suggests strong interfacial interactions between the deposited Pt NPs and ceria NRs.[28] This strong interaction may alter the crystallography and electronic structure of the Pt NPs and consequently affect the morphology of the catalyst, such as immobilizing the Pt NPs and preventing the Pt NPs from aggregation.

3.1.3 Morphology and chemical state study of Pt/ceria NPs. In contrast, for Pt/ceria NPs, the supported Pt NPs, which had similar sizes as ceria NPs, were observed to be dispersed among the ceria NPs (see Fig. 4). The sizes of ceria NPs were between 2 to 6 nm, similar to those of supported Pt NPs (2–5 nm). The Pt NPs were more spherical than the faceted "hemispherical" ones on ceria NRs. In Fig. 4a, the top right inset shows two HAADF-STEM images demonstrating the presence and distribution of ceria and Pt NPs where the Pt NPs appear brighter. The other inset image is a higher magnification of the boxed area where one Pt NP and one ceria NP were identified. The shape of Pt NPs also appeared to be less impacted by the ceria NPs. They did not seem to anchor well on the ceria supports and their shape appeared very much like the free standing particle (see Fig. 4b and c), suggesting insignificant atomic inter-diffusion between the Pt NPs and ceria support.

Similar to the case of Pt/ceria NRs, XPS Ce 3d spectrum analysis also indicated the presence of both Ce^{3+} and Ce^{4+} states (see Fig. 5a). XPS Pt 4f spectrum revealed that the dominant species in the Pt NPs of Pt/ceria NPs were Pt^0 (71%) (see fitting parameters in ESI Table S2†). These Pt particles also contained a significant proportion of Pt in the 2+ state (28%) (see Fig. 5b). No Pt^{4+} state fitting peaks were found necessary to reconstruct the Pt spectrum. The Pt–O–M species present in Pt/ceria NPs (1%) were considerably less than those in the Pt/ceria NRs, suggesting less interactions between Pt NPs and ceria NPs. Moreover, the much
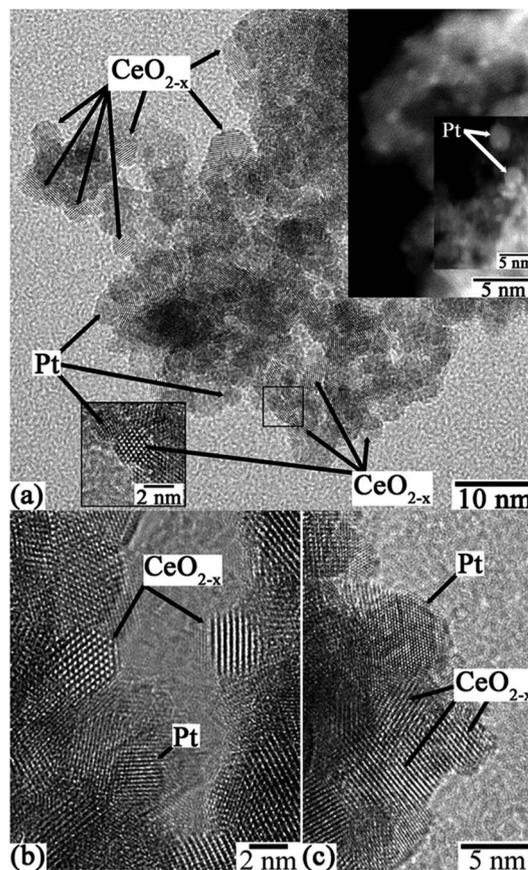

Fig. 4 (a, b and c) TEM images of the Pt/ceria NPs catalyst. The insets of 4a show two HAADF-STEM images.

larger proportion of Pt NPs in Pt^0 state suggests reduced charge transfers and weaker interactions between Pt NPs and ceria NPs when compared with the one in Pt/ceria NRs. The XPS analysis confirmed the data obtained from TEM experiments. With weaker interactions at the Pt/ceria interface, Pt nanocrystals easily agglomerate to form "spherically" shaped NPs.

3.2 Electrocatalytic performances of the Pt/ceria NRs and NPs electrodes towards methanol oxidation

The electrocatalytic activities of both Pt/ceria catalysts towards methanol oxidation were investigated using CV in 0.50 M KOH at
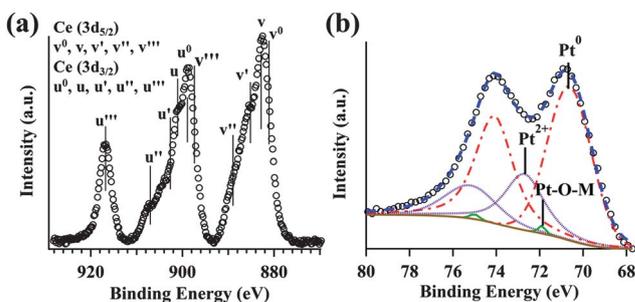

Fig. 5 X-ray photoelectron spectra and analysis of (a) Ce 3d and (b) Pt 4f data of Pt/ceria NPs.

room temperature. The CVs showed redox peaks in the region of −300 mV to 200 mV, corresponding to methanol oxidation and in agreement with reported data (Fig. 6a).[20,29,30] However, the current density per gram of Pt loading for the methanol electrooxidation with Pt/ceria NPs catalysts was about 2–5 folds larger than that with the Pt/ceria NRs catalysts from four data sets. This clearly reflects that the involvement of ceria NPs significantly increased the catalytic activity of the anode with the same Pt loadings. In addition, in Fig. 6a, the peak potential of anodic sweep for Pt/ceria NPs is −0.103 V *vs.* Ag/AgCl, while it is −0.082 V for Pt/ceria NRs. The peak potential shift indicates that the methanol oxidation on Pt/ceria NPs electrode is more active than that on Pt/ceria NRs electrode, which is consistent with the conclusion from our current density results.[20] The onset potential values of both catalysts also suggested that Pt/ceria NPs is a higher-performance anode catalyst since the onset potential is smaller than the one in Pt/ceria NRs. Thus, thermodynamically, the electrooxidation of methanol is more favorable with the Pt/ceria NPs catalyst. The onset potential values defined at 5% of the maximum peak current density for the methanol oxidation reaction performed with the catalyst coated anodes are shown in the forward sweep of the cyclic voltammograms obtained at a scan rate of 1 mV s^{-1} in Fig. 6b. Pt/ceria NPs exhibited an onset potential of −0.367 V *vs.* Ag/AgCl while that of Pt/ceria NRs is slightly higher at −0.333 V *vs.* Ag/AgCl.

The electrocatalytic activity of Pt/ceria catalysts is mostly attributed to the Pt^0 species of the Pt NPs. Pt^0 provides the most catalytically active sites for methanol electrooxidation.[31] The electrocatalytic performance of these catalysts suggests that Pt/ceria NPs had more catalytically active sites than Pt/ceria NRs. This is confirmed by the Pt active surface area measurements *via* hydrogen adsorption/oxidation potential region of the CV data (see ESI Fig. S1†). This finding also corroborates our XPS data that Pt/ceria NPs catalysts contain more Pt^0 states, but less oxidized Pt species. The higher catalytic activity of Pt/ceria NPs is also reflected indirectly by its lower electrical resistance in our EIS study. Nyquist plots were used to compare the resistance of charge transfer in both catalysts in 1.0 M MeOH/0.50 M KOH at an applied potential of −400 mV *vs.* Ag/AgCl. The charge transfer resistance was significantly smaller for the catalysts with ceria NPs than for the NRs catalysts (data not shown). This result allows us to conclude that the methanol electrooxidation in alkaline media is more favourable when using the Pt/ceria NPs catalyst than the one with ceria NRs support.

The catalytic activity of the catalyst-coated electrodes was also examined using chronoamperometry at an applied potential of −0.350 V *vs.* Ag/AgCl in 1.0 M methanol/0.50 M KOH solutions (Fig. 7). The observed current density for both catalysts decayed to *ca.* 0.2 mA mg^{-1} of Pt at 30 min. However, the Pt/ceria NPs exhibited slower decaying rate and slightly higher steady current density than those of Pt/ceria NPs. This observation confirms our CV results and is ascribed to the higher proportion of metallic Pt in the Pt/ceria NPs.

From the experimental results, the morphological differences between Pt/ceria NRs and NPs can be summarized in Scheme 1. The observed physical morphology and oxidation states of Pt NPs on the ceria NRs and NPs supports and their resulting catalytic activities can be attributed to the relative size differences and the degree of interactions between the Pt NPs and the ceria crystal plane facets. The ceria NRs provided relatively larger sized facets which allowed the deposited Pt NPs to spread and adopt an approximately faceted "hemispherical" morphology during the catalyst thermal activation step (left model in Scheme 1). In contrast, Pt NPs were found to attain more "spherical" shapes among the ceria nanoparticle aggregates. This was likely because, during the thermal activation process, the curvature-driven surface self-diffusion[32] of Pt atoms tended to reform NPs on jagged surfaces of aggregated ceria NPs (right model in Scheme 1). The several surface contact points between each Pt NP with
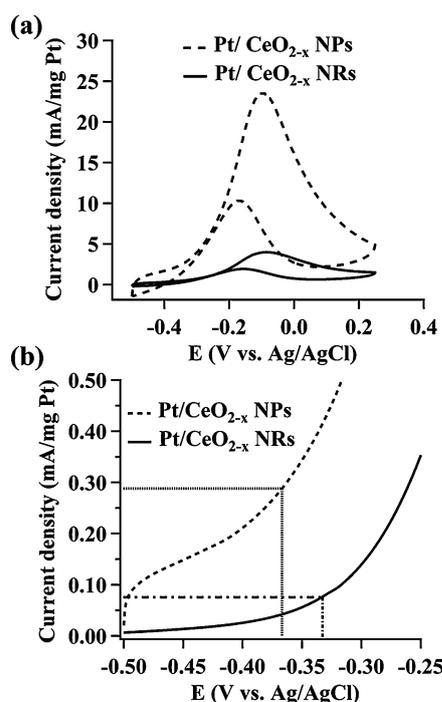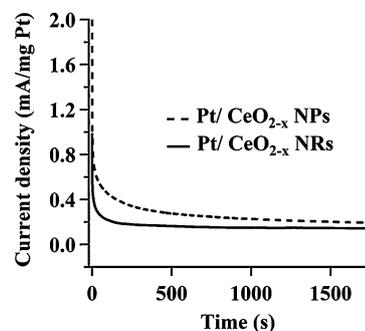

Fig. 6 (a) Cyclic voltammograms of Pt NPs on (solid) ceria NRs and (dotted) ceria NPs for alkaline methanol oxidation at a scan rate of 100 mV s^{-1} in 1.0 M MeOH/0.50 M KOH solutions. (b) Onset potential determination of Pt/ceria NRs and Pt/ceria NPs for alkaline methanol oxidation at a scan rate of 1 mV s^{-1}.

Fig. 7 Chronoamperometric responses of Pt/ceria NRs and Pt/ceria NPs catalysts performed at an applied potential of −0.350 V *vs.* Ag/AgCl in 1.0 M methanol/0.50 M KOH solutions.
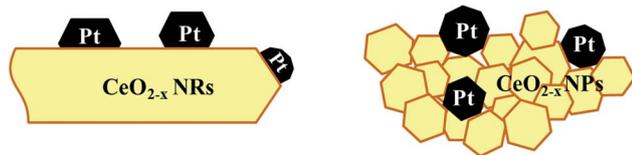
Scheme 1 Schematic of the postulated structural relationship between Pt NPs and ceria support for (right) Pt/ceria NRs and (left) Pt/ceria NPs. Pt NPs: black; ceria (CeO_{2-x}): yellow.

multiple ceria NPs of similar sizes may promote the Pt NPs to adopt more "spherical" shapes. The Pt NPs formed on ceria NRs contained more oxidized Pt species than those on ceria NPs. This implied that the ceria NRs had stronger interactions with supported Pt NPs than the case of ceria NPs. The strong metal support interactions were postulated to alter the morphology, increase the oxidation states of Pt and consequently decrease the availability of metallic Pt^0 sites and catalytic activity for methanol electrooxidation.

4. Conclusions

In summary, nanostructured ceria supports (NRs and NPs) were found to have significant effects on the chemical states of Pt NPs and hence their catalytic activities towards methanol oxidation in alkaline media. Pt NPs had a tendency to anchor strongly on ceria NRs due to their larger facets. However, Pt/ceria NRs showed higher concentrations of oxidized Pt species, therefore causing a decrease in their catalytic activity towards the electrooxidation of methanol in an alkaline media than in the case of Pt/ceria NPs. Our results suggest that though ceria has been widely explored as the promoter oxides for many metal-NPs-based electrocatalysts, the choice of morphology and size of the oxide promoter supports should also be carefully considered in the catalyst design.

Acknowledgements

Notes and references

1 M. Warshay and P. R. Prokopius, *J. Power Sources*, 1990, **29**, 193–200.

2 R. E. Martin and M. A. Manzo, *Proc. 23rd Intersoc. Energy Convers. Eng. Conf.*, 1988, vol. 2, pp. 301–304.

3 V. I. Matryonin, A. T. Ovchinikov and A. P. Tzedilkin, *Int. J. Hydrogen Energy*, 1997, **22**, 1047–1052.

4 V. S. Bagotzky and Y. B. Vassilyev, *Electrochim. Acta*, 1967, **12**, 1323–1343.

5 A. Hamnett, *Catal. Today*, 1997, **38**, 445–457.

6 A. M. Feltham and M. Spiro, *Chem. Rev.*, 1971, **71**, 177–193.

7 Z. L. Zhang, H. Song, S. B. Liu, Y. B. Li, X. G. Hao, D. H. Duan and Y. P. Sun, *Rare Met. Mater. Eng.*, 2012, **41**, 58–63.

8 R. S. Amin, R. M. A. Hameed, K. M. El-Khatib, M. E. Youssef and A. A. Elzatahry, *Electrochim. Acta*, 2012, **59**, 499–508.

9 N.-Y. Hsu, C.-C. Chien and K.-T. Jeng, *Appl. Catal., B*, 2008, **84**, 196–203.

10 M. M. P. Janssen and J. Moolhuysen, *Electrochim. Acta*, 1976, **21**, 869–878.

11 J. Zhao, L. Zhang, H. Xue, Z. Wang and H. Hu, *RSC Adv.*, 2012, **2**, 9651–9659.

12 B. Singh and E. Dempsey, *RSC Adv.*, 2013, **3**, 2279–2287.

13 F. Si, L. Ma, C. Liu, X. Zhang and W. Xing, *RSC Adv.*, 2012, **2**, 401–403.

14 S. A. Hayes, P. Yu, T. J. O'Keefe, M. J. O'Keefe and J. O. Stoffer, *J. Electrochem. Soc.*, 2002, **149**, C623–C630.

15 D. R. Ou, T. Mori, K. Fugane, H. Togasaki, F. Ye and J. Drennan, *J. Phys. Chem. C*, 2011, **115**, 19239–19245.

16 C. Bianchini and P. K. Shen, *Chem. Rev.*, 2009, **109**, 4183–4206.

17 E. H. Yu, K. Scott and R. W. Reeve, *J. Electroanal. Chem.*, 2003, **547**, 17–24.

18 H. B. Yu, J.-H. Kim, H.-I. Lee, M. A. Scibioh, J. Lee, J. Han, S. P. Yoon and H. Y. Ha, *J. Power Sources*, 2005, **140**, 59–65.

19 Q. Tang, Z. Mao, S. Ma and K. Huang, *RSC Adv.*, 2012, **2**, 11465–11471.

20 C. W. Xu and P. K. Shen, *Chem. Commun.*, 2004, 2238–2239.

21 N. J. Lawrence, J. R. Brewer, L. Wang, T.-S. Wu, J. M. Wells-Kingsbury, M. M. Ihrig, G. Wang, Y.-L. Soo, W. N. Mei and C. L. Cheung, *Nano Lett.*, 2011, **11**, 2666–2671.

22 D. Valechha, S. Lokhande, M. Klementova, J. Subrt, S. Rayalu and N. Labhsetwar, *J. Mater. Chem.*, 2011, **21**, 3718–3725.

23 D. Zhang, X. Du, L. Shi and R. Gao, *Dalton Trans.*, 2012, **41**, 14455–14475.

24 Z. Wu, M. Li and S. H. Overbury, *J. Catal.*, 2012, **285**, 61–73.

25 K. Fugane, T. Mori, D. R. Ou, A. Suzuki, H. Yoshikawa, T. Masuda, K. Uosaki, Y. Yamashita, S. Ueda, K. Kobayashi, N. Okazaki, I. Matolinova and V. Matolin, *Electrochim. Acta*, 2011, **56**, 3874–3883.

26 L. Cunci, C. V. Rao, C. Velez, Y. Ishikawa and C. R. Cabrera, *Electrocatalysis*, 2013, **4**, 61–69.

27 S. Deshpande, S. Patil, S. V. N. T. Kuchibhatla and S. Seal, *Appl. Phys. Lett.*, 2005, **87**, 133113.

28 Q. Fu, H. Saltsburg and M. Flytzani-Stephanopoulos, *Science*, 2003, **301**, 935–938.

29 S. S. Mahapatra and J. Datta, *Int. J. Electrochem.*, 2011, **2011**, 1–16.

30 E. Hao Yu, K. Scott and R. W. Reeve, *J. Electroanal. Chem.*, 2003, **547**, 17–24.

31 D. Santiago, G. G. Rodriguez-Calero, H. Rivera, D. A. Tryk, M. A. Scibioh and C. R. Cabrera, *J. Electrochem. Soc.*, 2010, **157**, F189–F195.

32 C. V. Thompson, *Annu. Rev. Mater. Res.*, 2012, **42**, 399–434.

Influence of nanostructured ceria support on platinum nanoparticles for methanol electrooxidation in alkaline media

Yunyun Zhou,[a] Christian L. Menéndez,[b] Maxime J.-F. Guinel,[b, c] Elizabeth C. Needels,[a] Ileana González-González,[b] Dichele L. Jackson,[a] Neil J. Lawrence,[a] Carlos R. Cabrera[b, *] and Chin Li Cheung[a, *]

[a] Department of Chemistry, University of Nebraska-Lincoln, Lincoln, NE 68588, USA.

[b] Department of Chemistry and NASA-URC Center for Advanced Nanoscale Materials, University of Puerto Rico, San Juan, Puerto Rico 00936-8377, USA.

[c] Department of Physics, College of Natural Sciences, University of Puerto Rico, San Juan, Puerto Rico 00936-8377, USA.

*Corresponding authors; e-mails: ccheung2@unl.edu; carlos.cabrera2@upr.edu

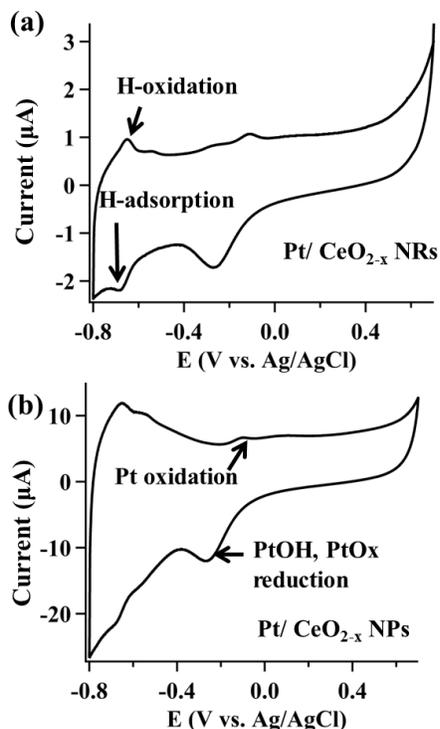**Electronic Supplemental Information**

Fig. S1 Cyclic voltammetry of (b) Pt/ceria NRs and (b) Pt/ceria NPs catalysts in 0.50 M KOH at 50 mV/s. The hydrogen adsorption and Pt oxidation and PtOH reduction are identified.

The Pt active surface area was determined by determining the charge in the hydrogen adsorption potential region.[1,2] Fig. S1 shows the typical CV curves of Pt/ceria in KOH solution. As it is well-known that ceria is not electroactive, peaks between -800 mV and -600 mV vs. Ag/AgCl are attributed to hydrogen adsorption. The large peak at -300 mV vs. Ag/AgCl on the cathodic scan is due to the reduction of Pt-OH and PtO_x to Pt^0. The peaks on the anodic scan are due to the formation of Pt hydroxide or oxides species from Pt^0.[3,4] Typical active Pt surface areas of Pt/ceria NPs catalyst deposited on the glassy carbon (GC) electrodes were about 0.017 cm^2 and that for the Pt/ceria NRs were about 0.0037 cm^2. Pt/ceria NPs exhibited 4 times more active Pt surface area than that of Pt/ceria NRs, which enabled Pt/ceria NPs to provide more active Pt sites to oxidize methanol in the solution and hence display higher catalytic current density per Pt loading.

Table S1 The fitting parameters for Pt 4f XPS data of Pt/ceria NRs.

Peak	Binding Energy (eV)	FWHM (eV)
Pt^0 ($4f_{7/2}$)	71.1	2.2
Pt-O-M ($4f_{7/2}$)	71.7	0.6
Pt^{2+} ($4f_{7/2}$)	72.8	1.7
Pt^{4+} ($4f_{7/2}$)	73.6	1.5
Pt^0 ($4f_{5/2}$)	74.6	1.7
Pt-O-M ($4f_{5/2}$)	75.4	0.6
Pt^{2+} ($4f_{5/2}$)	76.1	1.4
Pt^{4+} ($4f_{5/2}$)	77.1	1.3

Table S2 The fitting parameters for Pt 4f XPS data of Pt/ceria NPs.

Peak	Binding Energy (eV)	FWHM (eV)
Pt^0 ($4f_{7/2}$)	70.6	2.4
Pt-O-M ($4f_{7/2}$)	71.9	0.4
Pt^{2+} ($4f_{7/2}$)	72.7	2.1
Pt^0 ($4f_{5/2}$)	74.1	2.0
Pt-O-M ($4f_{5/2}$)	75.0	0.5
Pt^{2+} ($4f_{5/2}$)	75.2	2.8

References
1. J. M. D. Rodriguez, J. A. H. Melian and J. P. Pena, *J. Chem. Educ.*, 2000, **77**, 1195-1197.
2. F. G. Will, *J. Electrochem. Soc.*, 1965, **112**, 451-455.
3. S. Basu, ed., *Recent Trends in Fuel Cell Science and Technology*, Springer & Anamaya, 2007.
4. L. M. Pan, Z. Y. Zhou, D. J. Chen and S. G. Sun, *Acta Phys-Chim Sin.*, 2008, **24**, 1739-1744.